geosciences

MDPI

Article

Testing Semi-Automated Landforms Extraction Using Field-Based Geomorphological Maps

Salvatore Ivo Giano *, Eva Pescatore and Vincenzo Siervo

Dipartimento di Scienze di Base e Applicate, University of Basilicata, Campus Macchia Romana, Via Ateneo Lucano 10, I-85100 Potenza, Italy; eva.pescatore@alice.it (E.P.); vsiervo@gmail.com (V.S.)
* Correspondence: ivo.giano@unibas.it

Abstract: The semi-automated extraction of landforms using GIS analysis is one of the main topics in computer analyses. The use of digital elevation models (DEMs) in GIS applications makes the extraction and classification procedure of landforms easier and faster. In the present paper, we assess the accuracy of semi-automated landform maps by means of a comparison with hand-made landform maps realized in the Pleistocene Agri intermontane basin (southern Italy). In this study, landform maps at three different scales of 1:50,000, 1:25,000, and 1:10,000 were used to ensure a good level of detail in the spatial distribution of landforms. The semi-automated extraction and classification of landforms was performed using a GIS-related toolbox, which identified ~48 different landform types. Conversely, the hand-made landform map identified ~57 landforms pertaining to various morphogenetic groups, such as structural, fluvial, karst landforms, etc. An overlap of the two landform maps was produced using GIS applications, and a 3D block diagram visualization was realized. A visual inspection of the overlapping maps was conducted using different spatial scales of patch frames and then analyzed to provide information on the accuracy of landform extraction using the implemented tools.

Keywords: geomorphology; landforms extraction; landforms mapping; GIS application; southern Italy

Academic Editors: Luca Mao and Paul R. Eizenhöfer

Received: 21 November 2024
Revised: 27 January 2025
Accepted: 13 February 2025
Published: 17 February 2025

Citation: Giano, S.I.; Pescatore, E.; Siervo, V. Testing Semi-Automated Landforms Extraction Using Field-Based Geomorphological Maps. *Geosciences* **2025**, *15*, 70. https://doi.org/10.3390/geosciences15020070

1. Introduction

Earth's landforms are geomorphological features of landscape generated by the interplay of tectonic and climatic processes. The graphical representation of landforms using thematic maps is one of the main topics in geomorphological research [1–4]. Since the first hand-drawn geomorphological maps [5,6], technological progress has enabled users to extract and automatically produce landform maps by using DEM and GIS applications [7–9]. Modern applications in landform extraction and classification, such as spatial taxonomy, have been developed by various authors that have combined slope, relief, and profile classes in different ways resulting in five main types of landforms. They are generally classified as plains, tablelands, plains with hills or mountains, open hills and mountains, and hills and mountains [7–11]. The theoretical basis for land surface segmentation, which introduces the model of elementary forms as a primary concept in the interpretation of the genesis and evolution of landforms, was developed by Minar and Evans (2008) [8]. The basic principles of landform mapping are known as morphologic, genetic, chronologic, and dynamic, where the first is the most frequent and important, driving the three last types of classification [8,12]. The authors introduce three relief typologies based on the increasing landscape complexity: the elementary forms, the composite forms, and the land systems.

Several methods of semi-automated landform extraction and classification use multiscale approaches [13] or unsupervised nested mean algorithms [14] implemented using GIS tools, thus decreasing the amount of required user time and providing statistically based information on morphological features [1]. A method for the extraction and classification of landforms, based on the pattern recognition principle and named "Geomorphon", was recently proposed by Jasiewicz and Stepinski (2013) [15]. Using a mathematical vector framework, based on a triangulated irregular network (TIN) methodology, the basic terrain attributes were extracted from DEMs analyzing three real landform units [16]. Results were obtained from a comparison of different resolution DEMs and GIS applications were analyzed and discussed by Giano et al. (2020) [17]. The morphological adaptability of landforms to different landscapes was discussed by Brigham and Crider (2022) [18]. The authors compared the efficiency of a machine-learning algorithm with the interpretation of landforms by an expert geomorphologist, showing good correspondence of results. The original toolbox GIS implementation allowed Siervo et al. (2023) [19] to extract and classify several landforms in complex natural landscapes. A recent review that deals with the implementation and application of the different landform classifications using geospatial methods was proposed by Mashimbye and Loggenberg (2023) [20]. The theory of physically based geomorphometry was recently investigated by Minár et al. (2024) [4], improving land-surface segmentation and digital geomorphological mapping. The authors have enhanced the concept of elementary forms, moving towards a better morphogenetic interpretation of land-surface segmentation.

This paper tests the accuracy of the semi-automated extraction of landform maps obtained using GIS as proposed in [19], through a comparison with a field survey and hand-drawn landform maps [21]. The extraction of landforms was tested in the Agri intermontane basin, located in the southern Italian landscape (Figure 1a), where a detailed field survey geomorphological map was proposed by [21].

This field survey geomorphological map contains ~57 landforms, classified by the morphogenetic process and grouped into homogeneous morphogenetic classes. The semi-automated extraction of landforms enabled the classification of approximately 48 different types of landforms, based on the parameters set by the algorithm, as outlined in [19]. However, the current procedure does not provide genetic information about the identified forms as yet.

This paper aims to compare semi-automated and manual landform data to identify correspondences and explore parameters that could enhance automatic tools and also provide morphogenetic data. To achieve this goal, areas with significant geomorphological complexity were selected within the Agri intermontane basin, in southern Italy. In these areas, three different scales of landform maps—1:50,000, 1:25,000, and 1:10,000 scales—were utilized to visualize and emphasize various landform shapes. Data obtained from the semi-automated extraction of landforms were overlaid onto the field survey geomorphological map, georeferenced, and imported into GIS. A 5 m-resolution DTM was also utilized in the study, providing an additional analytical tool.

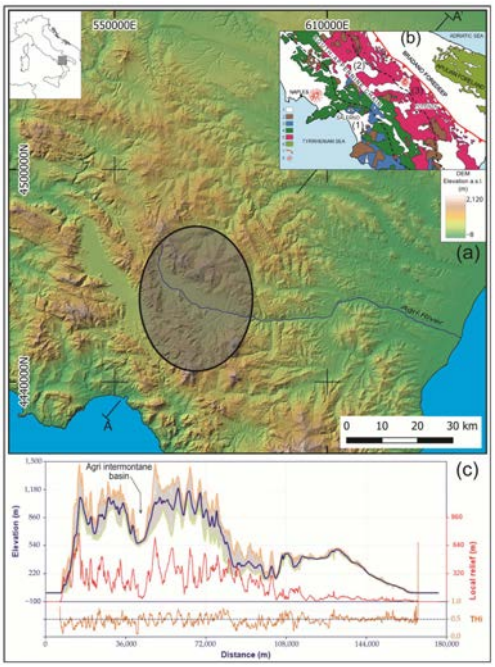

Figure 1. (**a**) Shaded relief showing the landscape of the southern Apennines; the grey ellipse box indicates the studied area. (**b**) Geological sketch map of southern Apennines. Legend: (1) Plio-Quaternary clastic and volcanic deposits, (2) Miocene syntectonic deposits, (3) Cretaceous to Oligocene ophiolite-bearing internal units, (4) Meso-Cenozoic shallow-water carbonates of the Apennine platform, (5) Lower-Middle Triassic to Miocene shallow-water and deep-sea successions of the Lagonegro units, (6) Meso-Cenozoic shallow-water carbonates of the Apulian platform, (7) thrust front of the chain, (8) volcanoes. Numbers (1), (2), and (3) indicate the inner, axial, and outer belt of the chain, respectively. (**c**) NE–SW-oriented topographic swath profile of southern Italy, from the Tyrrhenian to Adriatic coastlines. Maximum, minimum, and average elevations of the swath profile are represented by the orange, green, and blue lines, respectively; the red line indicates the local relief, and the yellow line at the bottom is the hypsometric integral (THi).

2. Geological and Geomorphological Background

The selected study area is located in the southern Apennine chain (Italy) and pertains to the upper sector of the Agri drainage basins (Figure 1a,b). It corresponds, from a geomorphological point of view, to the Agri intermontane basin, with a physical landscape covering ~620 km^2, with 17% consisting of plains, 37% hills, and 46% mountains. The climate has a mean temperature range of 10–18 °C and a mean annual precipitation range of 1000–850 mm from mountains to plain areas.

From a geological point of view, the fold-and-thrust belt of the southern Apennines is the result of the deformation of the Mesozoic–Cenozoic circum-Tethyan domains, which overlapped the foreland deposits of the Apulian Platform [22,23]. From a geographical point of view, the southern Apennine chain is composed of three main sectors, the inner, the axial, and the outer (numbered 1, 2, and 3, respectively, in Figure 1b), parallel to its NW–SE elongation axis. The inner sector is represented by the Tyrrhenian side, with its backbone mainly composed of Mesozoic shallow-water carbonates and Cretaceous-to-Miocene deep-sea pelagic successions. Mountain ranges are incised by transverse fluvial valleys driving the main rivers westward toward the Tyrrhenian Sea, producing narrow gorges sculpted within carbonate and siliceous rocks. Mesozoic to Cenozoic platform carbonate tectonic units, thrusted onto coeval deep-sea pelagic units, form the belt axial zone. Miocene flysch and clastic deposits of Pliocene thrust-top basins, both involved in contractional deformation, unconformably overlie these tectonic units [24] (Pescatore et al., 1999). The axial sector includes block-faulted ridges and morphostructures bounded by

fault scarp slopes [25–27]. They were displaced by Quaternary normal faults which are still active [27]. Pleistocene fault-related intermontane basins, filled with Quaternary fluvial and lacustrine deposits, are also present. The outer sector, which forms the eastern and southern sides of the southern Apennines, is composed of Cenozoic sandstones, marls, and clay forming the eastern imbricate fan of the orogenic wedge; it tectonically overlaps the Pliocene–Pleistocene clastic deposits of the Bradano foredeep or is locally buried by such sediments [28]. The outer zone displays a landscape with an average elevation lower than the axial belt zone and is characterized by a general passive north-eastward tilting. This is also supported by the orientation of major rivers that flow perpendicularly or obliquely to the elongation of the main tectonic structures. Middle-to-Late Pleistocene fluvial deposits are distributed along the main river valley sides, and both Holocene slope deposits and landslides are scattered throughout the area.

The asymmetric topographic profile of the southern Apennines chain, shown in a NW–SE-oriented swath topographic profile, exhibits the highest mountain peaks mainly located westwards of the regional watershed (Figure 1c). The asymmetry generates a greater length and a lower mean gradient in the Adriatic Sea sector of the chain compared to the Tyrrhenian Sea sector. As a consequence, rivers flowing towards the Tyrrhenian Sea show steeper channel gradients than those flowing towards the Adriatic and Ionian seas. In the axial sector of the chain, it is also possible to discriminate a topographic signature with a shorter wavelength that is linked to fault activity at intermontane basin flanks. These fault-related basins are surrounded by fault-related slopes as a consequence of Quaternary block faulting [25]. In this way, the basins are often bounded by flat-topped ridges representing three/four orders of erosional land surface carved into both Mesozoic-Cenozoic bedrock and Pliocene-Quaternary clastic sediments [21].

The Agri intermontane basin is a fault-related trough hosting the uppermost reach of the Agri River drainage basin (Figure 1a). The Agri River valley is N–S-oriented in the upper sector, changing to NW–SE and near W–E in the middle and lower sectors, respectively. It is about 30 km long and about 4 km wide, forming a NE–SW-oriented concave shape in plan view. The basin was developed during Quaternary times in the axial zone of the fold-and-thrust belt of the southern Apennines. The pre-Quaternary bedrock is composed of Mesozoic to Cenozoic shallow-water and slope carbonates of the Apennine Platform, which thrusted on the coeval pelagic successions of the Lagonegro units. The tectonic units crop out along the western and eastern sides of the valley. Furthermore, Oligocene to Miocene siliciclastic units (Albidona and Gorgoglione Fms) are present in the southeastern sector of the valley. The Pleistocene to Holocene clastic infill of the basin is formed of alluvial deposits about 500 m thick, which only crop out in the southern sector of the valley. The continental depositional sequence changes from fluvial (alluvial fan and plain) to lacustrine during time and space [29,30]. It is known as “Complesso val d’Agri” (sensu [29]), which is composed of three sedimentary units, the lower, the middle, and the upper, characterizing a coarsening upward depositional trend overall. The latter units, of the Middle Pleistocene, are mainly found in the central and southern sectors of the floor valley, where the Agri River and its tributaries have strongly incised about 200 m of the ancient depositional sedimentary top. The floor valley of the Agri basin is not vertically incised in the northern sector so information about the fill deposits comes mainly from boreholes and geophysical investigations. On both sides of the valley, Early to Late Pleistocene coarse-grained slope deposits crop out.

3. Materials and Methods

The extraction process of semi-automated landforms was realized considering the spatial dimension of the whole study area corresponding to ~620 km^2 (Figure 1a) and

the availability of different pixel resolution DEMs. The selected raster to be used for the area was the 5 m-resolution DEM, freely available at https://rsdi.regione.basilicata.it (accessed on 6 May 2024) The efficiency of 5 m-resolution DEM rather than 30 m- and 75 m-resolution ones has already been demonstrated in previous papers [17,19]. Furthermore, small-scale boxes were clipped into patch frames, as suggested by Li et al. (2022) [31]. The clipping procedure provides small-shaped areas of investigation and allows users to reduce both the computation and the time taken in the investigation. Conversely, large-shaped areas require a fast increase in computational demand, and the performance is slow and time-consuming. Starting from the semi-automated landforms map of the Agri intermontane basin at a 1:50,000 scale, two smaller-scale maps were produced at 1:25,000 and 1:10,000 scales, covering ~64 km^2 and 16 km^2, respectively. This was necessary to better visualize smaller landform typologies from both the semi-automated extraction procedure and the hand-made landform map. The semi-automated extraction tool for landforms runs using the ArcGIS 10.7 application permitting the extraction of 48 landforms. The landforms were classified based on six slope classes implemented in the tool, starting from the divide or interfluve of mountain ranges to the piedmont slope area or colluvial footslope (sensu [32–34], assuming a decrease in gradient slope. According to Siervo et al. (2023) [19], the six slope classes were classified starting from the lowest as follows: (i) Plain (0–5°), (ii) Toeslope (5–12°), (iii) Footslope (12–30°), (iv) Backslope (30–60°), (v) Shoulder (60–75°), and (vi) Summit-Free face (>75°). Furthermore, the slope classes were implemented in different altitudinal zones of the landscape, reflecting different dominant geomorphic processes acting on the mountain, hill, and plain zones. In the Italian physical landscape, the mountain altitudinal zones start above the mean altitude of 650 m a.s.l., the hill zone ranges from 650 m to 300 m a.s.l., and the plain zone is below the 300 m a.s.l. [35]. The same landform extracted in the three altimetric zones does not have the same morphological meaning because it could be generated by different geological and geomorphological processes. As a consequence, the same landform was differently named when located in a different altitudinal zone and generated by a different morphogenetic process. For example, a flat or low-angle and/or terraced surface could be assigned to a mass movement or landslide process in the hill zone, whereas in the mountain zone, it could be attributed to a depositional top surface or a planation surface. In addition, the flat or low-angle surfaces of the plain zone may be interpreted as fluvial/coastal plains or marine terraces. It is worth noting that the 48 extracted landforms pertain to the three altitudinal zones and each zone contains only 16 landforms. The altitudinal zones were numbered with a prefix listed as follows: 1–100 plain zone, 101–200 hill zone, and 201–300 mountain zone (Figure 2). Furthermore, each landform in the zone has a different color. Indeed, the color intensity increases from plain to hill and mountain, for similar landforms included in different altitudinal zones. Taking into account that the floor valley surface in the Agri intermontane basin is not higher than 530 m of elevation a.s.l., the landforms of the plain zone did not need to be extracted because they are present below 300 m of elevation. Only landforms of the hill and mountain zones were extracted and classified in the semi-automated landform map. The next step of the landform extraction was the definition of the Topographic Position Index (TPI) by applying a combination of Large (LN) and Small (SN) Neighborhoods according to the procedure proposed by Weiss (2001) [36] and implemented in GIS by Jenness (2006) [37]. The algorithm used in the application classifies the index into slope position and landform types according to the following equation:

$$TPIi = M_0 - \sum_{n-1} {}^{M_n}/_n$$

where M_0 is the elevation of the model point under evaluation, M_n is the elevation of the neighboring cells, and n is the total number of surrounding points applied in the evaluation [37]. Ridge areas are detected by positive TPI values whilst valley areas are detected by negative TPI values [36]. Conversely, values near zero TPI are representative of constant slopes or flat areas. The iterative process applied during the selection of the best TPI threshold value allowed [19] to suggest the best annulus criteria (Inner Radius and Outer Radius) for determining neighborhood size and shape. Values of 15(IR)–25(OR) in the Large neighborhood (LN), and 3(IR)–6(OR) in the Small neighborhood (SN) were used.

Figure 2. List of the extracted landforms. Colors discriminate different sectors of the landscape from plain to slope and top areas, whereas numbers were used to distinguish a similar landform classified in a different altimetric zone that can be plain, hill, and mountain.

The investigation of the Agri intermontane basin from a geomorphological point of view required the use of a field survey landform map showing the detailed distribution of landforms. In this paper, the geomorphological map edited by Giano (2016) [21] realized by aerial photo interpretation and field survey analyses, was used. The landforms map, firstly hand-drawn and then digitized using design software, contains many typologies of landforms, which were classified based on the main morphogenetic processes responsible for their formation (Figure 3). Each landform was drawn following its spatial and geometrical features such as aerial (e.g., surface of terraces), linear (e.g., fluvial channels), and punctual (e.g., karst holes). This means that polygons, lines, and points represent the graphical features used in the map representation. Furthermore, a different color discriminates each group of landforms. The landforms map shows the distribution of spatial, linear, and punctual landform types, including 57 different landforms grouped as follows: 12 structurally-controlled and tectonic landforms, 20 fluvial landforms, 8 karst landforms, 2 gravity-induced landforms, 3 glacial and periglacial landforms, 4 anthropogenic landforms, 4 depositional landforms, and 4 polygenetic landforms [21]. The final step involved the overlapping of shaded relief, semi-automated extracted landforms, and hand-made landform maps of the Agri intermontane basin, thus producing 3D landform maps. To avoid confusion among the colors representing landforms in the two maps, a 10 m difference in elevation between the two landform maps was introduced in the overlapping procedure. The visual inspection of the overlapped map allowed us to identify which extracted landforms could be linkable to the manually generated landforms and assess whether a different graphical representation was proposed by the two maps.

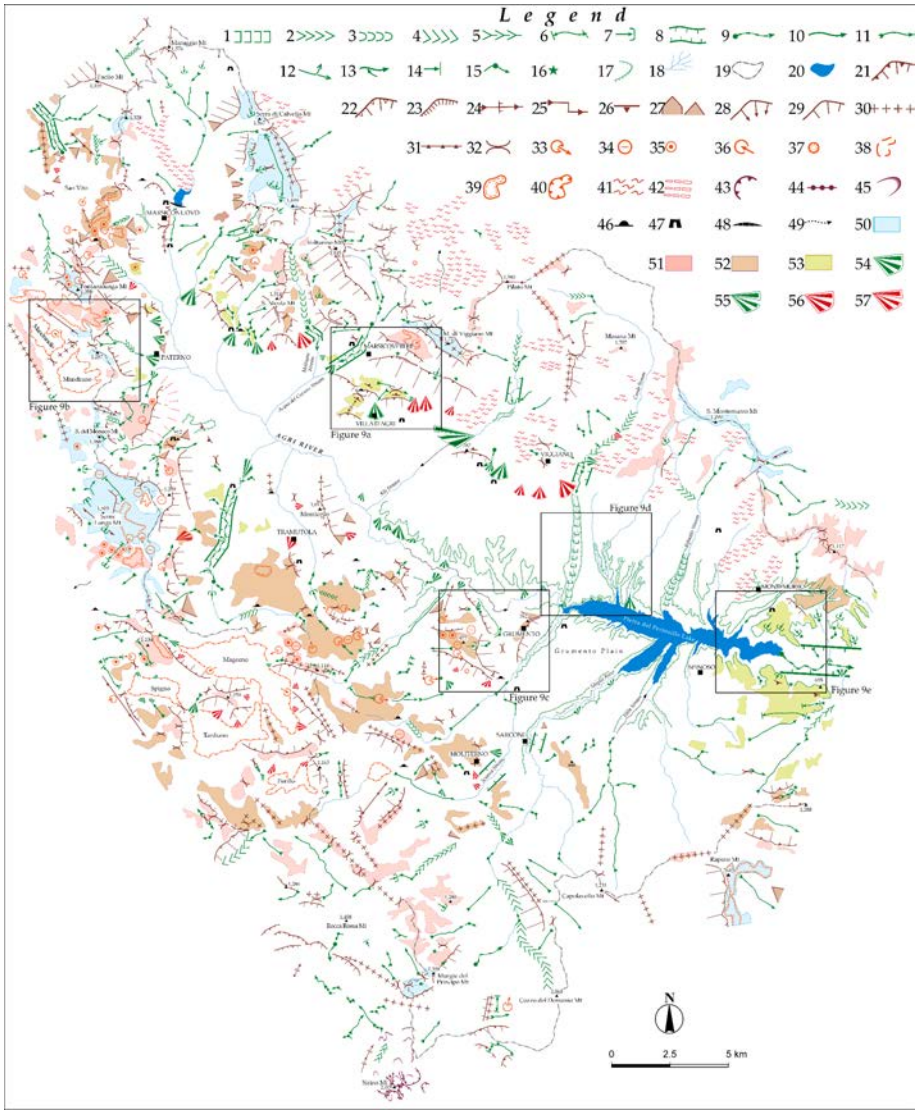

Figure 3. Hand-drawn geomorphological map of the Agri intermontane basin (modified after [21]). Legend: (1) flat-bottom valley; (2) V-shaped valley; (3) U-shaped valley; (4) asymmetric valley; (5) wine-glass valley; (6) relic valley; (7) hanging valley; (8) gorge; (9) transverse fluvial valley; (10) bedrock channel; (11) subsequent stream; (12) fluvial piracy; (13) counterflow confluence; (14) 90° confluence; (15) river elbow; (16) knickpoint; (17) edge of fluvial terrace; (18) main drainage network; (19) drainage divide; (20) water reservoir; (21) fault-related scarp; (22) fault-line scarp; (23) free face; (24) altimetric offset of ridge; (25) planar offset of ridge; (26) counter-side slope; (27) triangular or pentagonal facets; (28) structural slope; (29) backwearing slope; (30) straight symmetric or asymmetric ridges; (31) top-mountain alignment; (32) saddle; (33) open doline; (34) closed doline; (35) swallet hole; (36) blind valley; (37) cave; (38) uvala; (39) karst plain; (40) edge of polje floor; (41) landslide; (42) glacis; (43) glacial cirque; (44) arête; (45) moraine; (46) quarry; (47) archaeological site; (48) dam; (49) rectified stream; (50) palaeosurface Auctt. S1; (51) erosion surface S2; (52) erosion surface S3; (53) erosion surface S4; (54) alluvial fan; (55) entrenched alluvial fan; (56) talus debris fan; (57) entrenched talus debris fan. The box highlights details reported in the following figures.

4. Results

The recognition of different physical landscapes in the Agri basin was shown in three frames at a 1:10,000 scale containing the distribution of elevation and slope as main features of the landscape. In the first selected area, including the Marsicovetere and Villa d'Agri villages, the elevation ranges from 585 to 1678 m a.s.l. with a mean of 869 m and a standard deviation of 262 m. The latter value and the frequency distribution of elevation peaks

around 900 and 1300 m a.s.l. are indicative of the high dispersion of data which can be attributed to an extremely variable physical landscape. The relief of 1093 m, the average slope gradient of 15° and the standard deviation of 11° confirm a concave upward mountain slope with high potential energy (Figure 4a). The second area corresponds to the highland landscape of the Maddalena Ridge on the western side of the Agri basin. In this place, two Pleistocene tectono-karst basins, the Mandrano and Mandranello, are found [21]. The elevation ranges from 694 to 1358 m a.s.l. with a mean of 1075 m and a standard elevation of 111 m. A low value of standard deviation suggests a low-angle landscape, which is typical of relict planation surfaces. The relief of 664 m, the average slope gradient of 19° and the standard deviation of 8° suggest a low dispersion range of slope values and a moderate potential energy in the area, confirming the above interpretation (Figure 4b). The third area is located in the southern sector of the Agri basin and corresponds to the terraced surfaces of the Pleistocene Agri infill. The elevation ranges from 522 to 762 m a.s.l. with a mean of 590 m and a standard deviation of 40 m. The low value of the standard deviation suggests that elevation values are concentrated around the mean value of 590 m and thus the physical landscape could be interpreted as a flat and terraced surface. The relief of 240 m, the average slope gradient of 9° and the standard deviation of 10° indicate a flat topography with a dominance of low-angle values of slopes and low potential energy (Figure 4c). In summary, the frequency distribution of altitude and slope values are indicative of a dominant mountain to flat physical landscape with few hillslope features.

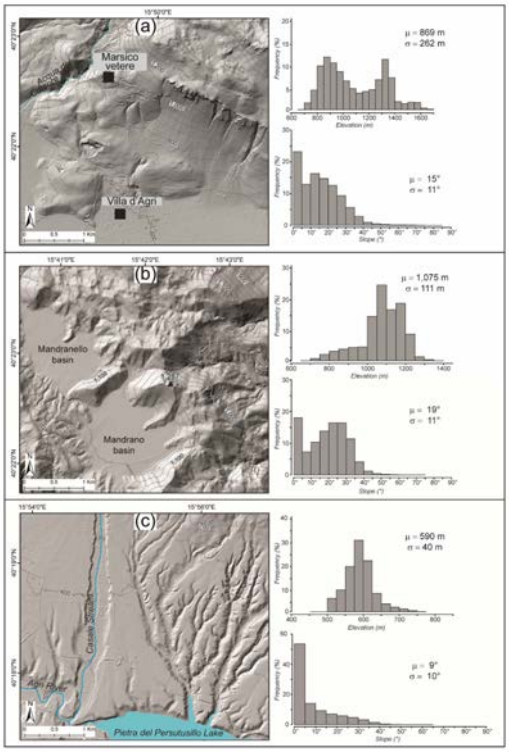

Figure 4. Shaded relief of the Marsicovetere (**a**), Mandrano (**b**), and Casale (**c**) areas. Histograms on the right side show the distribution of mean (μ) and standard deviation (σ) values for elevation and slope.

4.1. The Semi-Automated Landform Map of the Agri Basin

The extraction and classification of landforms in the Agri intermontane basin, realized using the GIS application, allowed us to detect fewer landforms distributed in the whole area than the 48 total landforms obtained by the standard GIS procedure. It is worth noting that the tool can recognize all landforms belonging to mountain, hill, and plain zones, and in the Agri basin, only the hill and mountain zones are present. The basin's lowest elevation

is higher than 530 m a.s.l. (Figure 5) so the landforms of the plain zone were not taken into account. Landform mapping of the entire Agri basin was realized at a 1:50,000 scale providing the first details on the landform distribution. However, this map does not allow users to discriminate landform detail.

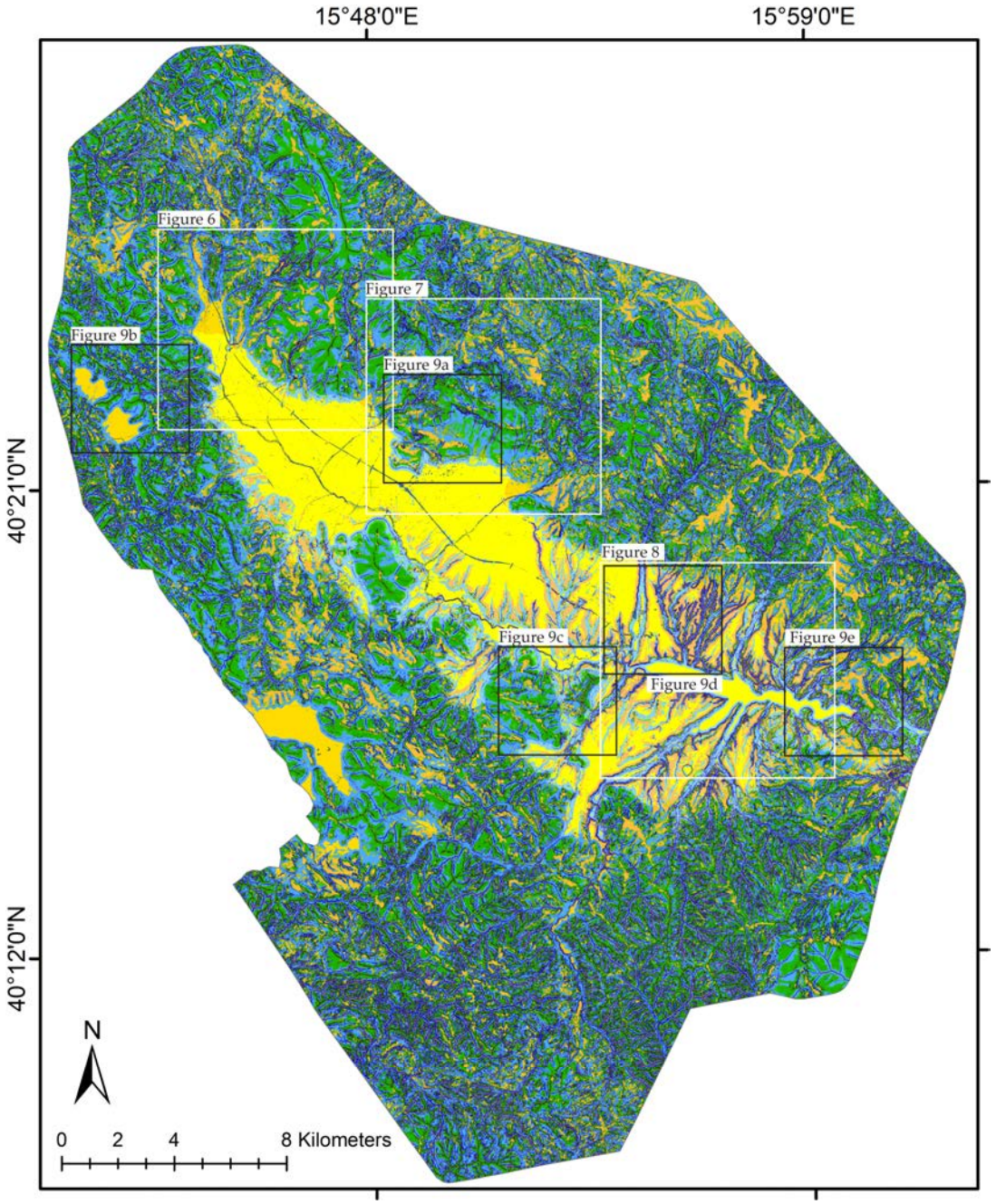

Figure 5. Landform map of the Agri intermontane basin extracted by the semi-automated procedure. See the color list in Figure 2 for landforms color legend. The box highlights details reported in the following figures.

To overcome this problem, three smaller patch frames, visualized at 1:25,000, were clipped in the DEM and were extracted by the landform map in Figure 5; they are representative of the upper, middle and lower sectors of the basin (Figures 6–8). The three maps show more details of the main elementary landform typologies. They are related to the valley sides in the upper reach (Figures 6 and 7) and the valley floor of the basin (Figure 8). In the first sector, the deeply incised stream and canyon landforms (number 201 in Figure 2)

are the most representative, corresponding to the Molinara, Acqua del Cursore, and Alli streams (Figures 6 and 7).

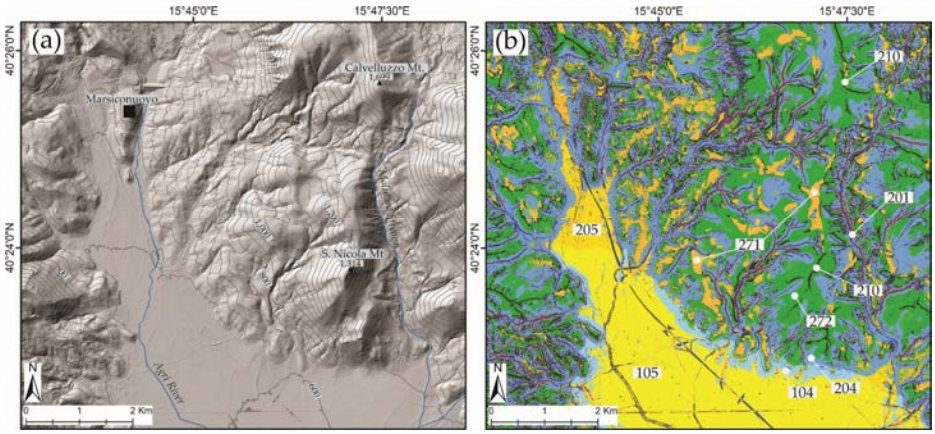

Figure 6. Detail of the upper sector of the Agri basin. (**a**) Shaded relief generated by a 5 m-resolution DEM and contour lines with 50 m-spacing of contour interval; (**b**) map of extracted landforms with landform identification number and colors listed in Figure 2.

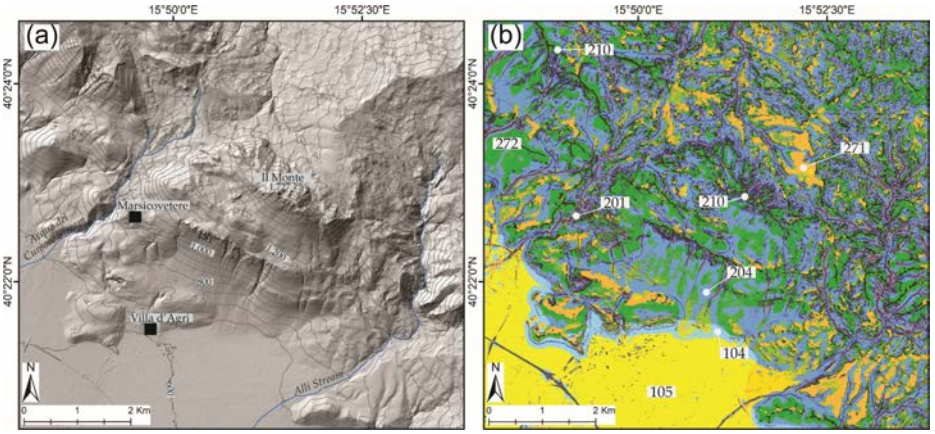

Figure 7. Detail of the middle sector of the Agri basin. (**a**) Shaded relief generated by a 5 m-resolution DEM and contour lines with 50 m-spacing of contour interval; (**b**) map of extracted landforms with landform identification number and colors listed in Figure 2.

Furthermore, flat and/or convex surface landforms (numbers 171 and 271 in Figure 2) are largely distributed along both the valley sides from the upper-to-lower sector. Mountain divide and ridge landforms (number 210 in Figure 2) are very evident and correspond to the small watersheds of the S. Nicola, Volturino, and Il Monte ridges. Finally, the topslope shoulder mountain landforms (number 272 in Figure 2) are scattered throughout the whole study area where relevant mountain slopes are found. The visual inspection also revealed an inaccurate extraction of piedmont mountain valleys with high-relief landforms (number 204 in Figure 2). This is evident in the southwestern slope of the Il Monte Mt (Figure 7), where landform areas are classified as 204 instead of 272. Conversely, the U-shaped valleys or infill valleys (numbers 104 and 204 in Figure 2) are well detected and can be related to the Casale, Rifreddo, Maglia, and Vella streams (Figure 8). Large spatial polygons are associated with valley floor landforms corresponding to the floodplain and fluvial terraces (numbers 105 and 205 in Figure 2) of the whole Agri basin (Figure 8). Although the upper reach floor valley corresponds to the present-day Agri River floodplain landform, from the Villa d'Agri village to the basin rim, the floor valley was vertically incised by the drainage network and then the sedimentary top forms fluvial terraces (Figure 8). In fact, a

well-developed drainage network in the interfan area between the Casale and Rifreddo streams was extracted and visualized. Small- and deep-incised streams form a dendritic fluvial pattern, and the flat and convex terraced surfaces landforms are clearly evident (Figure 8).

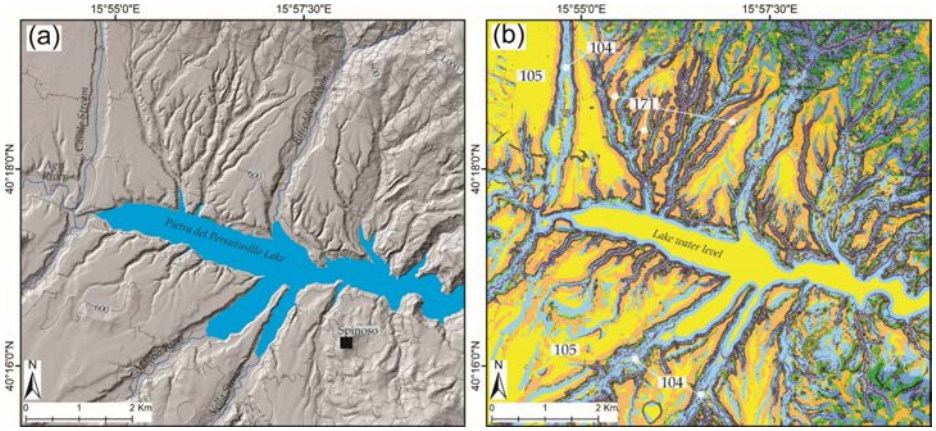

Figure 8. Detail of the lower sector of the Agri basin. (**a**) Shaded relief generated by a 5 m-resolution DEM and contour lines with 50 m-spacing of contour interval; (**b**) map of extracted landforms with landform identification number and colors listed in Figure 2.

Several geomorphic features of landforms are not clearly visible at the 1:25,000 scale, so it was necessary to produce more detailed landform maps at a 1:10,000 scale (Figures 9 and 10). The mountain divide and ridge landforms (number 210 in Figure 9a,b), located close to the Marsicovetere village, are represented by a continuous alignment of pixels, despite a step in the elevation of the divide. Furthermore, in mountain ridges, such as the Mandrano area, it is possible to observe greater physical continuity of the mountain divide line landforms. Piedmont slope areas (204), low-angle or convex surfaces (271), and topslope shoulder landforms (272) are the most spatially distributed landforms, which dominate the slopes in the mountain landscape (Figure 9a–c). Canyons and deep-incised stream landforms (201), corresponding to the main hydrographic network, are well defined and continuous; particularly, the canyon landforms reflect the fluvial thalwegs in the high-incised fluvial valleys (Figure 9d,e). The algorithm recognized the flat surfaces of the floor valley basin and the flat terraced surfaces (105) of the basin located in the lower sector of the basin close to Grumento Nova village and Pietra del Pertusillo Lake (Figures 8 and 9c). Furthermore, two mountain suspended floor plain landforms (205), which correspond to the Mandrano and Mandranello endorheic basins were detected (Figures 4b and 9b), representing tectono-karst landforms distributed at the mountain top of Maddalena Ridge [21]. In this case, the mountain divides are well-evidenced by the algorithm producing continuous lines reflecting the watershed of the structurally-controlled ridges. However, the tool does not seem to have well worked in this area, where extremely irregular topographic shapes are found. Considering the more erodible lithologies compared to the other ridges, the high fragmentation of landforms forming a puzzle-shape can be attributed to the presence of mass movements such as landslide landforms. It is important to point out that the semi-automated extraction method allows us to discriminate between the shape of the landscape based on its slope gradient but not the process responsible for its formation. Also, close to Marsicovetere village, unclear landforms were automatically extracted; nevertheless, in the piedmont area close to Villa d'Agri village, large and moderate shapes of alluvial fans can be observed (Figure 9a). Conversely, in the foothill areas of Monte San Nicola (Figure 6), where small fans are distributed, the algorithm was not able to recognize landforms; in fact, these areas were classified as U-shaped valley landforms.

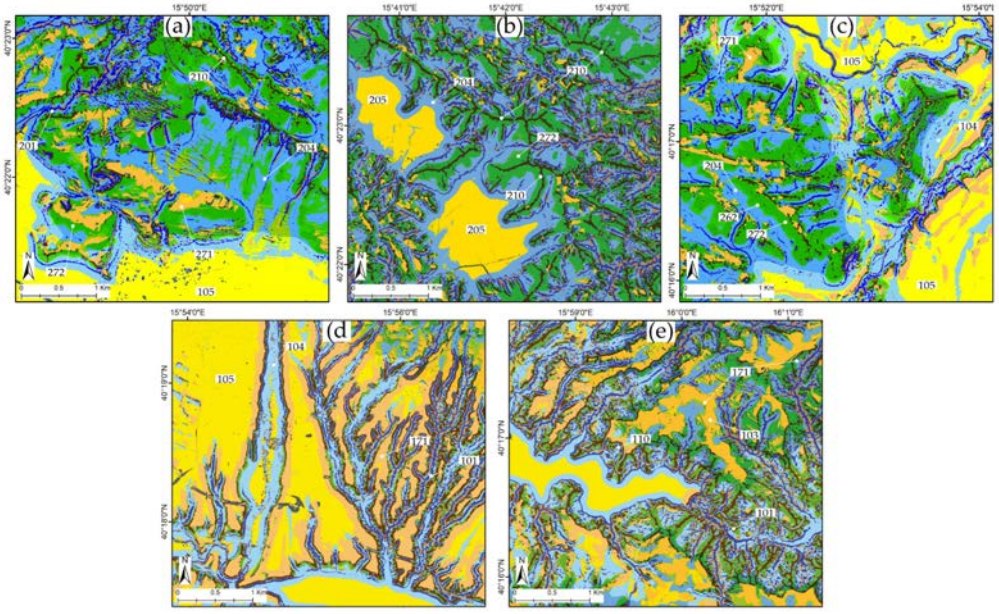

Figure 9. Details of the extracted landforms map at a 1:10,000 scale with landform identification numbers and colors as in Figure 2. Location of sites: (**a**) Marsicovetere, (**b**) Maddalena Ridge, (**c**) Grumento nova, (**d**) Casale, and (**e**) Pertusillo.

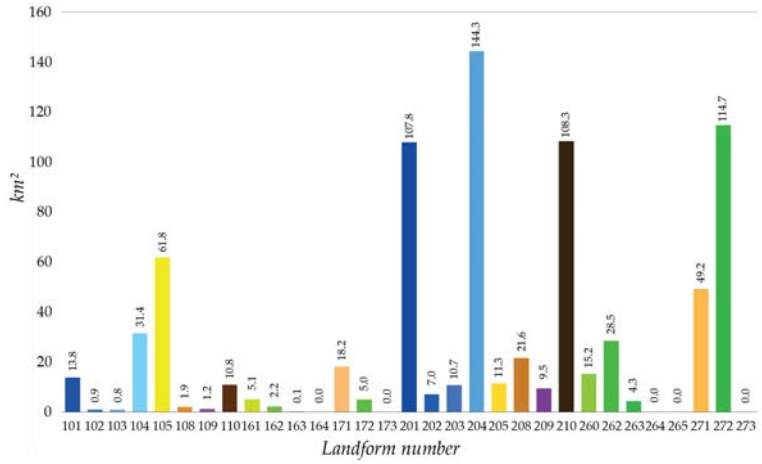

Figure 10. Spatial extension diagram in km^2 of the extracted landforms in the Agri basin.

A grouped column histogram was used to produce a statistical analysis of the landform distribution related to each single landform and illustrate their spatial extension expressed in km^2 (Figure 10). The statistical analysis revealed that the U-shaped mountain valley landform (204) is the largest one, occupying the largest surface extension in the Agri intermontane basin and reaching a value of 144.3 km^2. That landform can be added to a similar landform such as the U-shaped hill valley (104), which occupies 31.4 km^2, thus reaching a total surface extension of 175.7 km^2. There are other landforms showing high spatial values, such as the shoulder mountain slopes (272) with 114.7 km^2, the mountain divides (210) with 108.3 km^2, and the canyons and deep-incised streams (201) with 107.8 km^2, which represent the more frequent landforms of the Agri Basin (Figure 10). The flat hill surface landform (105) has low spatial distribution, but is still significant, with 61.8 km^2, and the mountain low-angle surface landform (271) has a distribution of 49.2 km^2. Smaller spatial distributions are those of the small-incised stream (101), hill fluvial divides (110), convex and/or flat upper hill surfaces (171), upstream drainages (203), mountain suspended floor plains (205), local ridges (208), low toeslope mountains (261), reaching spatial extensions

ranging between 10 and 20 km^2. Finally, landforms with spatial dimensions smaller than 10 km^2 are scattered across the whole Agri basin area.

4.2. The Field-Based Geomorphological Map of the Agri Basin

In [21], which deals with the detection and the hand-drawing of the main landforms sculptured in the Agri intermontane basin, seven groups of landforms modelled by different surface processes acting on both the Mesozoic and Cenozoic bedrock and the Pleistocene clastic deposits were listed. The landforms provide information about the long- to short-term landscape evolution since Pliocene times. Based on the main morphogenetic processes acted in the past, 57 landforms were collectively recognized and grouped as follows: (1) structurally-controlled and tectonic; (2) fluvial; (3) karst and fluvio-karst; (4) gravity-induced mass movement; (5) glacial and periglacial; (6) anthropogenic; (7) polygenic (Figure 3). Some of these groups of landforms are shown within small patch frames at 1:25,000 and 1:10,000 scales, which are representative of the whole basin area. The frames were extracted and reinterpreted from the geomorphological map of the Agri intermontane basin edited by Giano (2016) [21].

Structurally-controlled and tectonic landforms are largely distributed in both sides of the valley of the Agri basin and represent positive fault-bounded mountain blocks which are bounded by several kilometers of roughly rectilinear mountain fronts. Structural landforms such as fault-related scarps, saddles, straight ridges, and triangular facets are the more representative, whereas the others are less abundant (Figure 11a–e). Geological and geomorphological information are also congruent with fault scarps and fault-line scarp landforms [26,38], mainly oriented N110°–130° and N150°–180°. The faulting activity was responsible for the creation of several hundred meters of morphological offsets along the side-valley of the Agri basin. The compound fault scarp of the Monte di Viggiano morphostructure evidence the coeval existence of more than one landform: (i) a replacement slope and (ii) a free face remnant (Figure 11a). In the northern sector of the western side valley, the N–S oriented box-fold of the Serra di Calvello mountain block contains an example of a convergent landform represented by triangular facets. The altimetric and planar offset of ridges, symmetric/asymmetric straight ridges, and top-mountain alignment landforms point out rectilinear faulted structures that are interrupted by morphological saddles in some places. Fluvial landforms including shaped valleys and linear features are represented by the V-shaped and U-shaped valleys of the Casale and Molinara streams, respectively. Wine-glass and flat-bottom valleys are other landforms that are less widely distributed in the basin. Relict and hanging valleys, marking the occurrence of past base levels, are found at the Calvelluzzo Mt. and the Pietra del Pertusillo site. The vertical incision generated by the Agri River and its tributaries was responsible for transverse fluvial valleys and gorge formation (Figure 11e). The deeper gorges of the basin are represented by the Pietra del Pertusillo—forming the southern threshold of the intermontane basin, the Cavolo, and the Acqua del Cursore streams. Bedrock channels and subsequent streams, counterflow confluences, river elbow, and knickpoint landforms are some of the morphotectonic markers distributed in the basin. In the southern sector of the basin, fluvial terraces tens of meters high and incised in the clastic infill deposits, are present.

On the platform carbonate rocks of the Monti della Maddalena tectonic units, the largest and well-shaped karst landforms were modelled (Figure 11b). They are located in the right-side valley, where closed and open dolines contain small swallet holes, whereas uvala and karst plain landforms represent the main karst landforms of the area. In fact, the polje of Mandrano, Mandranello, Spigno, and Tardiano are the larger landforms and reach about 4 km^2 width in the Magorno polja. They are distributed at different elevations up to 1000 a.s.l. and on the top of the Maddalena mountain ridges. Endokarst landforms are quite

rare in the basin, and only at the Castel di Lepre site, a cave system horizontally extending for about 145 m was explored. Remnants of glacial landforms distributed from about 1400 to 2000 m of elevation a.s.l. are still preserved at the Mt. Sirino massif and in the surrounding areas. In fact, there are relicts of glacial cirques that are separated by thin arêtes landforms. A north-facing cirque contains a preserved tarn landform known as Remmo Lake. Moraine deposits are found in the surrounding areas of the massif which are formed of sub-angular and heterometric clasts with a silty-sandy matrix produced by calcareous and siliceous successions of the local geological bedrock. They were produced during several generations of glacial episodes and allowed [39] to recognize the last glacial maximum boundary placed at 1250 m a.s.l. Polygenetic landforms were sculptured by fluvial processes, in combination with dissolution processes on carbonate rocks, thus forming several generations of low-angle land surfaces. The highest and oldest erosion summit surface is also known as Palaeosurface Auctt. and three lower and younger planation surfaces, S2, S3, and S4, distributed at different elevation a.s.l. within the Agri catchment basin are the low-angle or flat terraced surfaces landforms.

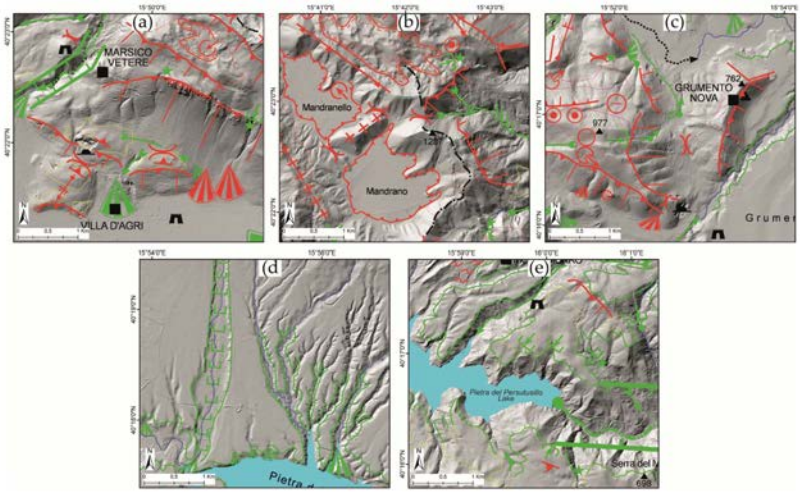

Figure 11. Details of the hand-drawn landform map at a 1:10,000 scale overlapped on the hill shade. Location of sites: (**a**) Marsicovetere, (**b**) Maddalena Ridge, (**c**) Grumento nova, (**d**) Casale, and (**e**) Pertusillo. See Figure 3 for the legend of landform symbols. See Figure 3 for landforms simbology.

Finally, the Agri intermontane basin contains many anthropogenic landforms because it has experienced human settlements since the Neolithic age, reaching its maximum population density in the Bronze Age [40]. However, the best-preserved evidence comes from the Hellenistic-Lucanian period and the Roman age, where towns were built on the valley floor. Among them, the Colonia Romana of *Grumentum* represents the best expression of the anthropogenic activity in the basin. Fairly important are the two dams of Marsico Nuovo and Pietra del Pertusillo. The first is located in the uppermost basin and was built at the end of the last century whilst the second is found in the southernmost basin and was built in the middle of the last century.

5. Discussion

We overlaid landform maps, created using both manual and semi-automated extraction methods, on a 3D digital terrain model for comparison. This process enabled us to identify shapes that are clearly recognizable in both types of maps (best fitting), as well as those that are not easily distinguishable (poorly fitting). Among the best fitting results, geomorphological features can be identified by individual shape or by a combination of two shapes. The first is represented by (i) 101 and 201 in Figure 2, representing the hydrographic network (18 in Figure 3); (ii) 110 and 210 in Figure 2, corresponding to ridges (30 and 31

in Figure 3). The former is represented by (i) 101 associated with (a) 104 corresponding to flat-bottom valley (1 in Figure 3), and (b) 171 corresponding to hanging valley (7 in Figure 3); (ii) 201 associated with (a) 204 representing U-shaped valley (3 in Figure 3), and (b) 271 corresponding to knickpoint (16 in Figure 3); (iii) 162 associated to 262, and 172 associated to 272 corresponding to slopes (28 and 29 in Figure 3). Among the combinations of two shapes, a separate discussion concerns the shapes identifying the flat surfaces, 105 and 205 in Figure 2. These can correspond to non-incised or incised flat surfaces depending on whether they are associated with the shapes 104 and 204, respectively, or with 171 and 271, respectively. The first can be related to floodplains or generic floor plains. The former can be related to terraces (17 in Figure 3) or erosion surfaces. Below are some examples of what has been described and observed in the sample areas.

- *Polygonal features*
  - The flat surfaces, namely, the floodplain and terraces of the Agri River and the floor depositional plain of the small endorheic basins, are clearly identifiable (Figure 12a–c; Figure 13a). In Figure 12b, the red lines corresponding to the edge of the poljes floor (hand-drawn map) fit well with the suspended floor plain and piedmont slope valley landforms of the extracted map. The green line corresponding to the edges of the terraces on the hand-drawn map (17 in Figure 3) is identified in the automated procedure as landform number 171, and fits well in the extracted map (Figures 12a and 13a).
  - Concerning the karst landforms (33–40 in Figure 3), only the large tectonic-karst landforms, such as uvala and polje, were well-detected by the semi-automated procedure. Small karst landforms, such as small doline, swallet hole, cave and blind valley landforms, were not recognized.
  - The four orders of erosion surfaces identified in the hand-drawn map (50 to 53 in Figure 3) were partially detected in the semi-automated extraction process, which showed significant partitioning and fragmentation (Figures 12b–d and 13b). These surfaces are remnants of more or less continuous and engraved areas that the human operator interprets and reports as unique polygons. In the automatic extraction process, these polygons correspond to flat and convex shapes (171 and 271), associated with slope shapes (272). This association generates a visual fragmentation, suggesting that automatic extraction is not well-suited, in this case. The question concerning the recognition and delimitation of relict and engraved erosion surfaces has already been outlined by many authors [2,15,41] and the semi-automated procedure seems not to be able to detect this morphological feature. The reason could be attributed to the physical complexity of this kind of landscape feature, which contains diverse landforms. A variation in the range of the TPI window could be applied using an iterative procedure, only to this kind of landform, with the purpose of verifying the best values that are able to detect them.

- *Linear features*
  - The extracted hydrographic network (101 and 201) is appropriate and satisfactory, and fits well with the data reported in the hand-drawn map. The channel's network was clearly evidenced in the upstream valley areas and became less distinct in the downstream ones. The low hierarchical order of streamlines was well-emphasized in the mountain drainage basins, whilst the high order streamlines were less pronounced or sometimes absent. In the lower reach of entrenched fluvial valleys, such as the Molinara and Rifreddo streams (left-side valley) and the Maglie and Vella streams (right-side valley), the small- or deep-incised stream-

lines were not extracted and are only shown in their upstream valley sectors (Figure 13a). Shapes 101 and 201 include also subsequent streams, bedrock channels, and symmetrical and asymmetrical valleys.

- The mountain and hill divides (110 and 210) were well-evidenced and congruent with the one presented in the hand-drawn map, also including the straight symmetric or asymmetric divides (30 in Figure 3). In this last case, the information relating to the linearity of the shape, indicative of possible tectonic control, is not highlighted.
- Flat-bottom and U-shaped valley landforms (1 and 3 in Figure 3) required a merging of two extracted landforms (101 + 104 and 201 + 204) to be identified. In Figures 12c and 13a, the Molinara and Casale streams are examples of U-shaped and flat-bottom valleys landforms, respectively.
- Hanging fluvial valley and knickpoint landforms required the merging of two landforms (101 + 171 and 201 + 271) to be identified. Where a transition from low-angle or convex surface to small/deep-incised stream landforms occurs, the hanging valley and knickpoint landforms located at the edge of scarps can be detected (Figure 12c,d).
- Structural and backwearing slopes, represented as linear features in the hand-drawn map (28 and 29 in Figure 3) required the merging of two landforms (162 + 172 and 262 + 272) to be identified. These shapes include also fault scarp and fault-line scarp (21 and 22 in Figure 3). The crest line of fault-related scarps, and structural and backwearing slopes are present in the Volturino and Il Monte mountain ridge (Figures 7 and 12c,d).

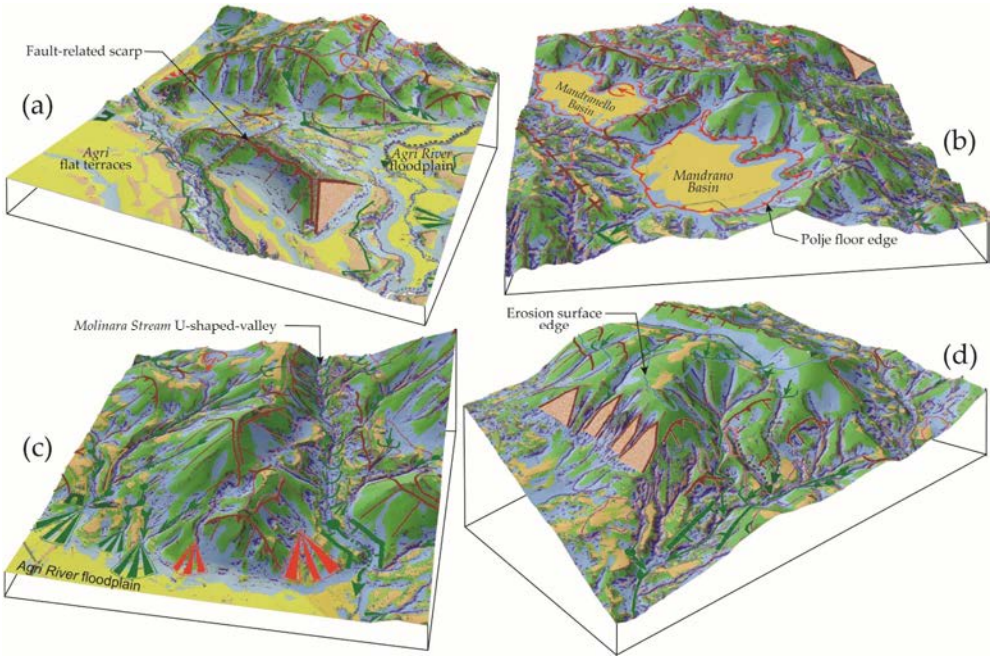

Figure 12. 3D overlay maps of different sites in the Agri basin showing a merge between the hand-drawn and extracted landform maps. The frames are related to Grumento Nova (**a**) in Figure 9c, Maddalena mountain ridge (**b**) in Figure 9b, Molinara Stream valley (**c**) in Figure 6b, and Serra di Calvelluzzo mountain ridge (**d**) in Figure 6b. See Figures 2 and 3 for landforms colors and symbology.

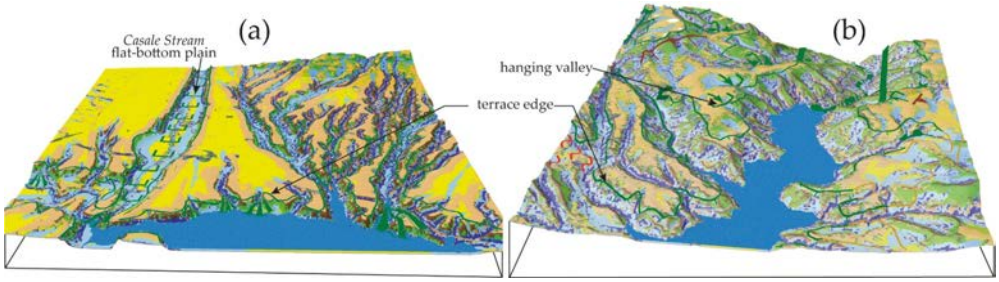

Figure 13. 3D overlay maps of different sites in the Agri basin showing a merge between the hand-drawn and extracted landform maps. The frames are related to Casale Stream valley (**a**) in Figure 9d and the Agri basin rim (**b**) in Figure 9e. See Figures 2 and 3 for landform colors and symbology.

The upper reaches of the left side of the Agri basin feature various noteworthy landforms, including subsequent streams, pentagonal facets, fault-related scarps, U-shaped valleys, erosion surfaces, gorges, and backwearing slopes (Figures 14a,b and 15a). The basin also showcases two distinct flat surface landforms: the non-incised and the incised, and terraced floor valley (Figure 14c,d). The Mandrano and Mandranello polje, swallet holes, dolines, and erosion surfaces are the dominant karst landforms in the right-side valley of the Agri basin (Figure 15b,c).

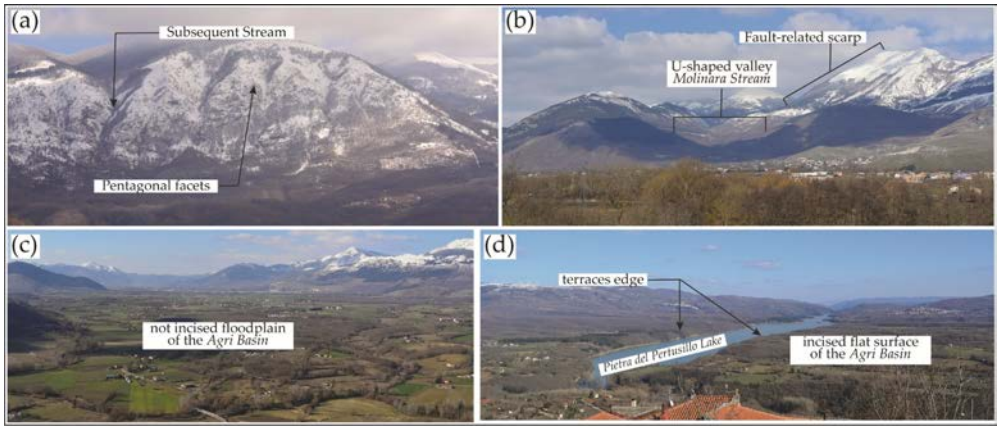

Figure 14. Panoramic view of some landforms detected in the Agri basin. Serra di Calvelluzzo mountain ridge (**a**), Molinara Stream valley (**b**), middle-to-upper sector of the non-incised floodplain of the Agri basin (**c**), and southern sector of the Agri basin incised by the Agri River and its tributaries (**d**).

Landforms extracted by the semi-automated procedure and by the manual approach in the five sampled areas of Marsicovetere, Mandrano, Grumento Nova, Casale, and Pertusillo (Figures 9 and 11) were plotted in a scatter class diagram (Figure 16) to compare them individually. The Marsicovetere and Mandrano sites contain top-related and slope-related landforms, respectively, such as drainage divide (210), topslope shoulder mountain (272), and piedmont slope area (204) landforms. Grumento Nova evidenced low toeslope mountain (262) whereas Casale and Pertusillo showed flat hill and terraced surface (105) landforms, among others.

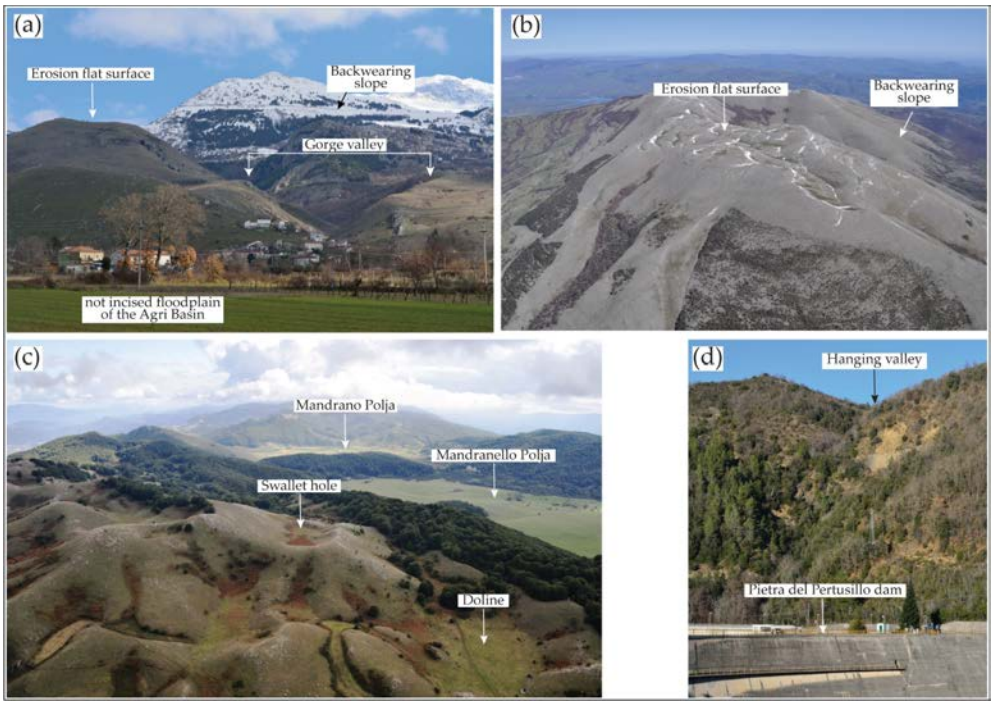

Figure 15. Panoramic view of some landforms detected in the Agri basin. Madonna di Viggiano mountain ridge (**a**), Raparo mountain ridge (**b**), Maddalena mountain ridge (**c**), Pietra del Pertusillo dam (**d**).

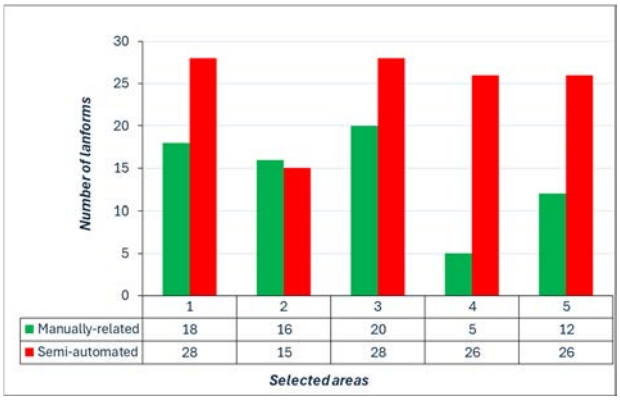

Figure 16. Diagram of manually detected vs. semi-automated landforms at the Marsicovetere (1), Maddalena Ridge (2), Grumento nova (3), Casale (4), and Pertusillo (5) sites.

The diagram shows that the semi-automated landforms are always more abundant than the manually detected ones in all the sampled sites, except in the Mandrano area where landforms are equal in number. Hence, the GIS application was able to extract more landform typologies than the field survey investigation, making the process less time consuming for users.

The main difficulties regarding this study involved selecting the study parameters (such as TPI, scale, and DTM resolution) and the fragmentation of some forms that are clearly visible in the field survey geomorphological map.

Various tests were conducted using different value ranges to determine the most suitable parameters for effectively highlighting the landforms in the analyzed territory. Although it is obvious that the scale to be used must best highlight the landforms, its definition requires trial and error because the landform's representativeness also depends on its size. The same is true for the definition of the TPI parameters, which are strictly dependent on the type of landscape. When dealing with areas that exhibit significant

morphological diversity, it may be necessary to find a compromise by experimenting with several attempts. This is particularly relevant regarding the identification of erosion surfaces that are not distinctly defined and consist of incised, relict portions of various sizes.

6. Conclusions

In the Agri intermontane basin, the landforms map extracted using a semi-automated procedure was overlapped with a manually generated landforms map to check the correspondence between the identified shapes.

The overlapping demonstrated that only some typologies of landforms recognized by the semi-automated procedure correspond to the manually recognized ones. This applies to the drainage network and the divides when using a single extracted landform or when merging two extracted landforms (Figure 17). Conversely, many landforms of the hand-made map were poorly detected or not detected by the semi-automated procedure of extraction, highlighting the need for improvement of the tool in future developments. Based on this study, the main issues that require improvement are i) the fragmentation of relict erosion surfaces and ii) differentiation between low-angle areas related to river terraces, marine terraces or sinkhole bottoms.

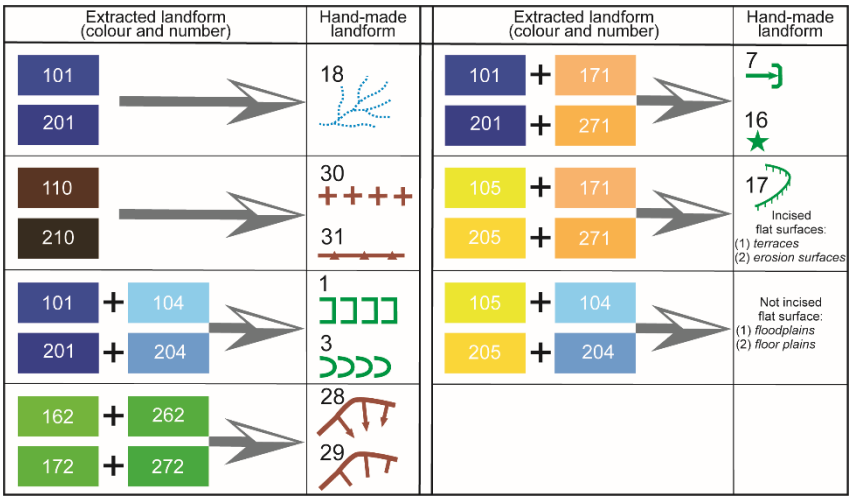

Figure 17. Correspondence between the manually generated and semi-automated typologies of landforms.

The question concerning the recognition and delimitation of relict and engraved erosion surfaces has already been outlined by many authors [2,15,41] and the semi-automated procedure seems unable to detect this morphological feature. The reason could be attributed to the physical complexity of this kind of landscape feature, which may contain diverse landforms. A variation in the range of the TPI window could be applied using an iterative procedure, only to this kind of landform, with the purpose of verifying the best values that are able to detect them. Regarding low-angle areas associated with terraces, to enhance the automatic extraction tool, it is essential to incorporate additional parameters that enable subsequent form differentiation. This could involve using lithological information to differentiate between fluvial, marine, or carbonate deposits, as well as measures of the polygon's sphericity or ellipticity to identify certain karst features. The goal of this discrimination is not to achieve automatic identification, but rather to highlight data that require further human verification.

Finally, the question regarding the differentiation between structural and backwearing slopes, as well as between faults and fault-line scarps, currently appears to be closely

related to human activity. This issue could be better understood by incorporating additional parameters, such as the attitude of the strata and the linearity of the derived shapes.

The semi-automatic extraction methods take into account the shape of the landform and not the process responsible for its formation. For this reason, many landform types, resulting from different morphological processes, will not be discriminated in an extracted landforms map but represented together. Indeed, it is important to specify that the semi-automated method of landform extraction should not replace traditional methods such as field survey or aerial-photo interpretation. It represents support in the recognition of geomorphological features and ensures the mapping of large areas with relatively low time and cost requirements, leaving less space for the user's subjectivity. There is no doubt that in recent years important and notable steps forward have been made in the field of new technologies, especially in the field of AI. Increasingly complex algorithms capable of processing multiple data are continuously being created, updated, and implemented. Although we expect that in the not-too-distant future, we will arrive at the automatic extraction of landforms and their characterization from a genetic point of view, we believe that human oversight is still fundamental and irreplaceable, at least for the time being.

Author Contributions: Conceptualization, S.I.G., E.P. and V.S.; methodology, S.I.G. and V.S.; software, S.I.G. and V.S.; validation, S.I.G., E.P. and V.S.; formal analysis, S.I.G., E.P. and V.S.; investigation, S.I.G., E.P. and V.S.; resources, S.I.G., E.P. and V.S.; data curation, S.I.G., E.P. and V.S.; writing—original draft preparation, S.I.G. and E.P.; writing—review and editing, S.I.G. and E.P.; visualization, S.I.G., E.P. and V.S.; supervision, S.I.G., E.P. and V.S.; project administration, S.I.G.; funding acquisition, S.I.G. All authors have read and agreed to the published version of the manuscript.

Funding: This research was funded by FFABR 2018, granted to S.I. Giano.

Data Availability Statement: The original contributions presented in this study are included in the article. Further inquiries can be directed to the corresponding author(s).

Conflicts of Interest: The authors declare no conflicts of interest. The funders had no role in the design of the study; in the collection, analyses, or interpretation of data; in the writing of the manuscript; or in the decision to publish the results.

References

1. Evans, I.S. General geomorphometry, derivatives of altitude, and descriptive statistics. In *Spatial Analysis in Geomorphology*; Chorley, R.J., Ed.; Methuen: London, UK, 1972; pp. 17–90.
2. Evans, I.S. Geomorphometry and landform mapping: What is a landform? *Geomorphology* **2012**, *137*, 94–106. [CrossRef]
3. Burrough, P.A.; McDonnel, R.A. *Principles of Geographical Information Systems*; Oxford University Press: Oxford, UK, 1998; pp. 1–350.
4. Minár, J.; Drăgut, L.; Evans, I.S.; Feciskanin, S.; Gally, M.; Jenčo, M.; Popov, A. A Physical geomorphometry for elementary land surface segmentation and digital geomorphological mapping. *Earth-Sci. Rev.* **2024**, *248*, 104631. [CrossRef]
5. Horton, R.E. Erosional development of streams and their drainage basins; hydrophysical approach to quantitative geomorphology. *Bull. Geol. Soc. Am.* **1945**, *56*, 275. [CrossRef]
6. Strahler, A.N. Quantitative Analysis of Watershed Geomorphology. *Trans. Am. Geophys. Union* **1957**, *38*, 913–920. [CrossRef]
7. Evans, I.S. *An Integrated System of Terrain Analysis and Slope Mapping. Final Report on Grant DA-ERO-591-73-60040*; University of Durham: Durham, UK, 1979; p. 192.
8. Minar, J.; Evans, I.S. Elementary forms for land surface segmentation: The theoretical basis of terrain analysis and geomorphological mapping. *Geomorphology* **2008**, *95*, 236–259. [CrossRef]
9. Blaszctynski, J.S. Landform characterization with geographic information systems. *Photogram. Engin. Rem. Sens.* **1997**, *63*, 183–191.
10. Hammond, E.H. Analysis of properties in landform geography: An application to broadscale landform mapping. *Ann. Assoc. Am. Geogr.* **1964**, *54*, 11–19. [CrossRef]
11. Dikau, R.; Brabb, E.E.; Mark, R.K.; Pike, R.J. Morphometric landform analysis of New Mexico. *Zeitsch. Für Geomorph. Supplem.* **1995**, *101*, 109–126.

12. Speight, J.G. A parametric approach to landform regions. In *Progress in Geomorphology: Papers in Honor of D.L. Linton*; Brown, E.H., Waters, R.S., Eds.; Alden Press: London, UK, 1974; Volume 7, pp. 213–230.
13. Wood, J. The Geomorphological Characterisation of Digital Elevation Models. Ph.D. Thesis, University of Leicester, Leicester, UK, 1996. Available online: https://www.proquest.com/openview/13f37e44dfd15ee5661ae23edef43c68/1?pq-origsite=gscholar&cbl=51922&diss=y (accessed on 6 May 2024).
14. Iwahashi, J.; Pike, R.J. Automated classifications of topography from DEMs by an unsupervised nested-means algorithm and a three-part geometric signature. *Geomorphology* **2007**, *86*, 409–440. [CrossRef]
15. Jasiewicz, J.; Stepinski, T.F. Geomorphons-A pattern recognition approach to classification and mapping of landforms. *Geomorphology* **2013**, *182*, 147–156. [CrossRef]
16. Hu, G.; Xiong, L.; Lu, S.; Chen, J.; Li, S.; Tang, G.; Strobl, J. Mathematical vector framework for gravity-specific land surface curvatures calculation from triangulated irregular networks. *GIScience Remote Sens.* **2022**, *59*, 590–608. [CrossRef]
17. Giano, S.I.; Danese, M.; Gioia, D.; Pescatore, E.; Siervo, V.; Bentivenga, M. Tools for Semi-automated Landform Classification: A Comparison in the Basilicata Region (Southern Italy). In Proceedings of the International Conference on Computational Science and Its Applications, Cagliari, Italy, 1–4 July 2020. [CrossRef]
18. Brigham, C.A.P.; Crider, J.G. A New Metric for Morphologic Variability Using Landform Shape Classification via Supervised Machine Learning. *Geomorphology* **2022**, *399*, 108065. [CrossRef]
19. Siervo, V.; Pescatore, E.; Giano, S.I. Geomorphic analysis and semi-automatic landforms extraction in different natural landscapes. *Environ. Earth Sci.* **2023**, *82*, 128. [CrossRef]
20. Mashimbye, Z.E.; Loggenberg, K. A Scoping Review of Landform Classification Using Geospatial Methods. *Geomatics* **2023**, *3*, 93–114. [CrossRef]
21. Giano, S.I. Geomorphology of the Agri intermontane basin (val d'Agri-Lagonegrese National Park, Southern ltaly). *J. Maps* **2016**, *12*, 639–648. [CrossRef]
22. Patacca, E.; Scandone, P. Geology of the Southern Apennines. *Boll. Soc. Geol. Ital. Spec. Issue* **2007**, *7*, 75–119.
23. Rizzo, G.; Cristi Sansone, M.T.; Perri, F.; Laurita, S. Mineralogy and petrology of the metasedimentary rocks from the Frido Unit (southern Apennines, Italy). *Period. Mineral.* **2016**, *85*, 153–168.
24. Pescatore, T.; Renda, P.; Schiattarella, M.; Tramutoli, M. Stratigraphic and structural relationships between Meso-Cenozoic Lagonegro basin and coeval carbonate platforms in southern Apennines, Italy. *Tectonophysics* **1999**, *315*, 260–286. [CrossRef]
25. Giano, S.I.; Schiattarella, M. Age constraints and denudation rate of a multistage fault line scarp: An example from Southern Italy. *Geochronometria* **2014**, *41*, 245–255. [CrossRef]
26. Bavusi, M.; Chianese, D.; Giano, S.I.; Mucciarelli, M. Multidisciplinary investigations on the Grumentum Roman acqueduct (Basilicata, southern Italy). *Ann. Geophys.* **2004**, *47*, 1791–1801.
27. Barchi, M.; Amato, A.; Cippitelli, G.; Merlini, S.; Montone, P. Extensional tectonics and seismicity in the axial zone of the southern Apennines. *Boll. Soc. Geol. It.* **2007**, *7*, 47–56.
28. Casnedi, R. La fossa bradanica: Origine, sedimentazione e migrazione. *Mem. Soc. Geol. It.* **1988**, *41*, 439–448.
29. Di Niro, A.; Giano, S.I.; Santangelo, N. Primi dati sull'evoluzione geomorfologica e sedimentaria del bacino dell'Alta Val d'Agri (Basilicata). *Studi Geol. Camerti. Nuova Ser.* **1992**, *1*, 257–263.
30. Zembo, I. Stratigraphic architecture and quaternary evolution of the Val d' Agri intermontane basin (Southern Apennines, Italy). *Sediment. Geol.* **2010**, *223*, 206–234. [CrossRef]
31. Li, S.; Li, K.; Xiong, L.; Tang, G. Generating terrain data for geomorphological analysis by integrating topographical features and conditional generative adversarial networks. *Remote Sens.* **2022**, *14*, 1166. [CrossRef]
32. Dalrymple, J.; Long, R.; Conacher, A. A hypothetical nine-unit land- surface model. *Zeitsch. Für Geomorph.* **1968**, *12*, 60–76.
33. Young, A. *Slopes*; Oliver & Boyd: Edinburgh, UK, 1972; p. 288.
34. Bloom, A.L. Geomorphology. In *A Systematic Analysis of Late Cenozoic Landforms*; Prentice Hall: Englewood Cliffs, NJ, USA, 1991; p. 532.
35. ISTAT Circoscrizioni Statistiche. *Metodi e Norme 1958, Serie C n. 1, 1–239*; AbeteEd.: Roma, Italy.
36. Weiss, A.D. Topographic position and landforms analysis. In *Poster Presentation*; ESRI User Conference: San Diego, CA, USA, 2001.
37. Jenness, J. Topographic Position Index (tpi_jen.avx) Extension for ArcView 3.x, v. 1.2. Jenness Enterprises. 2006. Available online: http://www.jennessent.com/arcview/tpi.htm (accessed on 10 July 2022).
38. Brancaccio, L.; Cinque, A.; Sgrosso, I. Forma e genesi di alcuni versanti di faglia in rocce carbonatiche: Il riscontro naturale di un modello teorico. *Rend. Acc. Sc. Fis. Mat.* **1979**, *46*, 1–21.
39. Boenzi, F.; Palmentola, G. Nuove osservazioni sulle tracce glaciali nell'Appennino Lucano. *Boll. Com. Glac. It.* **1972**, *20*, 9–52.

40. Tarlano, F.; Bogdani, J.; Priore, A. Upper Agri valley (Basilicata) between geomorphology and ancient settlements. In Proceedings of the 3 International Landscape Archaeology Conference (LAC), Rome, Italy, 17–20 September 2014.
41. Smith, M.J.; Paron, P.; Griffiths, J.S. *Geomorphological Mapping. Methods and Application. Development in Earth Surface Processes*; Elsevier Press: Amsterdam, The Netherlands, 2011; Volume 15, pp. 1–612.